Paper 75

©Civil-Comp Press, 2012
Proceedings of the Eleventh International Conference
on Computational Structures Technology,
B.H.V. Topping, (Editor),
Civil-Comp Press, Stirlingshire, Scotland

Damage Localisation in Composite Laminated Plates using Higher Order Spatial Derivatives

P. Moreno-García[1], H. Lopes[2], J.V. Araújo dos Santos[3] and N.M.M. Maia[3]
[1] INEGI, Instituto de Engenharia Mecânica e Gestão Industrial, Porto, Portugal
[2] ESTIG, Instituto Politécnico de Bragança, Portugal
[3] IDMEC/IST, Instituto Superior Técnico, Lisboa, Portugal

Abstract

A new vibration based damage localisation method relying on differences of third and fourth order spatial derivatives of modal displacements of composite laminated plates is proposed in this paper. The damage is simulated by decreasing the laminate stiffness of specific finite elements. Since the displacement fields of the damaged plate are discrete, they are differentiated using higher order finite differences. The modal displacement fields of the undamaged plate are obtained using the Ritz method and, therefore, the spatial derivatives are computed analytically. Parametric studies relating the number of measured degrees of freedom to the quality of the damage localisations are carried out. The results of the present method are compared with the results obtained with an extension of the well-known rotation and curvature methods. It was found that higher order derivatives, in particular fourth order derivatives, are very promising for damage localisation in composite laminated plates.

Keywords: damage localisation, finite element method, Ritz method, higher order spatial derivative, laminated plate.

1 Introduction

The use of vibration characteristics as a mean to detect, locate and quantify structural damage has been reported extensively in the literature [1, 2]. One of the most well established methods was proposed by Pandey et al. [3] and is based on the differences of mode shape curvatures of undamaged and damaged beams. The curvatures are computed by applying the second order central finite difference formula to the measured displacements fields. According to Abdo and Hori [4] one may also use the differences in the rotation of mode shapes to localise damage. However, these methods are prone to errors arising from the finite difference itself and the propagation of the measurement errors which are always present in experimental data. In order to cope with this problems, some improvements on these methods and similar ones, such as the damage index [5] and the frequency response functions curvature [6] methods, have been reported [7–15]. Also, the use of higher order derivatives for the damage identification in beam-like structures has been previously reported [16–18].

The development of a method for localisation of damage in composite laminate plates, based on differences of third and fourth order spatial derivatives of modal displacement fields, i.e. mode shapes, is presented in this paper. The modal displacement fields of the undamaged plate are obtained using the Ritz method. Since this method describes the displacement field as a series expansion, a direct analytical computation of the spatial derivatives, which is more accurate than the computation with finite differences, is possible. The damaged plate is modeled by finite elements. Therefore, the modal displacement field obtained needs to be differentiated using numerical techniques. In the present work, higher order finite differences are used. Contrary to most techniques found in the literature, with the proposed method it is possible to compute the modal displacement fields derivatives and, therefore, the damage indicators at the edges of the plate by applying backward and forward finite differences.

2 Damage Localisation Methods

2.1 Undamaged and Damaged Plate Models

2.1.1 Ritz Method for Undamaged Orthotropic Laminated Plates

Bearing in mind the Kirchhoff assumptions [19], the strain energy of a plate of volume V is given by

$$U = \frac{1}{2}\int_V (\sigma_x\epsilon_x + \sigma_y\epsilon_y + \sigma_{xy}\epsilon_{xy})dV \tag{1}$$

where σ_x, σ_y, σ_{xy} are the stresses and ϵ_x, ϵ_y, ϵ_{xy} are the strains. After considering the constitutive relations of an orthotropic plate, the kinematic assumptions, integrating in the z direction, and taking into account only the maximum amplitude of vibration $w(x,y)$, Equation (1) defines the maximum strain energy:

$$U_{\max} = \frac{1}{2}\int_A \left\{ D_{11}\left[\frac{\partial^2 w(x,y)}{\partial x^2}\right]^2 + D_{22}\left[\frac{\partial^2 w(x,y)}{\partial y^2}\right]^2 \right. \\ \left. +4D_{66}\left[\frac{\partial^2 w(x,y)}{\partial x \partial y}\right]^2 + 2D_{12}\frac{\partial^2 w(x,y)}{\partial x^2}\frac{\partial^2 w(x,y)}{\partial y^2}\right\} dA \tag{2}$$

where $D_{ij} = \displaystyle\int_{-h/2}^{h/2} Q_{ij}^{(k)} z^2 dz$ are the laminate stiffnesses, $Q_{ij}^{(k)}$ being the plane stress reduced stiffnesses of the k-th lamina and h the thickness of the plate [19]. In Equation (2), A denotes the in-plane surface area of the plate.

The kinetic energy of the plate in terms of the in-plane displacements $u(x, y, t)$ and $v(x, y, t)$, out-of-plane displacement $w(x, y, t)$ and the material density ρ, is given by

$$T = \frac{1}{2}\int_V \rho\left\{\left[\frac{\partial u(x,y,t)}{\partial t}\right]^2 + \left[\frac{\partial v(x,y,t)}{\partial t}\right]^2 + \left[\frac{\partial w(x,y,t)}{\partial t}\right]^2\right\} dV \tag{3}$$

Considering the Kirchhoff assumptions and after integrating in the z direction, Equation (3) reduces to

$$T = \frac{1}{2}\int_A \rho h\left[\frac{\partial w(x,y,t)}{\partial t}\right]^2 dA \tag{4}$$

Since the plate is vibrating with harmonic motion at an angular frequency ω, the maximum kinetic energy is given by

$$T_{\max} = \frac{1}{2}\omega^2\int_A \rho h[w(x,y)]^2 dA \tag{5}$$

In the Ritz method one assumes the solution for the maximum amplitudes $w(x, y)$ to be of the form

$$w(x,y) = \sum_{m=1}^{M}\sum_{n=1}^{N} W_{mn}X_m(x)Y_n(y) \tag{6}$$

where $X_m(x)$ and $Y_m(y)$ are functions compatible with the boundary conditions, M and N are the number of terms in the series and W_{mn} is a set of parameters to be determined.

The Ritz method relies on the minimisation of the functional $T_{\max} - U_{\max}$ with respect to the parameters W_{kl} [20, 21]:

$$\frac{\partial(T_{\max} - U_{\max})}{\partial W_{kl}} = 0 \quad \text{with} \quad k = 1, \ldots, M \quad \text{and} \quad l = 1, \ldots, N \tag{7}$$

Therefore, by replacing Equation (6) in Equations (2) and (5), applying Equation (7) and performing the necessary mathematical manipulations one gets

$$\begin{aligned}
&\sum_{m=1}^{M}\sum_{n=1}^{N}\left\{\int_A (\rho h X_k X_m Y_l Y_n) dA\right\} W_{mn}\omega^2 \\
&-\sum_{m=1}^{M}\sum_{n=1}^{N}\left\{\int_A \left[D_{11}\frac{d^2X_k}{dx^2}\frac{d^2X_m}{dx^2}Y_lY_n + D_{22}X_kX_m\frac{d^2Y_l}{dy^2}\frac{d^2Y_n}{dy^2}\right.\right. \\
&\qquad +D_{12}\left(\frac{d^2X_k}{dx^2}X_mY_l\frac{d^2Y_n}{dy^2} + X_k\frac{d^2X_m}{dx^2}\frac{d^2Y_l}{dy^2}Y_n\right) \\
&\qquad \left.\left. +4D_{66}\frac{dX_k}{dx}\frac{dX_m}{dx}\frac{dY_l}{dy}\frac{dY_n}{dy}\right] dA\right\} W_{mn} = 0
\end{aligned} \tag{8}$$

This expression defines an eigenvalue problem of size $M \times N$:

$$[K][W] = [M][W][\omega^2] \tag{9}$$

where $[K]$ and $[M]$ are matrices containing the stiffness and the inertial characteristics, respectively, and $[W]$ and $[\omega^2]$ are matrices containing the parameters W_{mn} and the circular natural frequencies ω. The matrix $[\omega^2]$ is diagonal and $[W]$ is a full matrix.

The assumed functions used in this work are the ones proposed by Gartner and Olgac [22] for the analysis of beams and present a greater numerical stability than the usual characteristic functions:

$$X_m(x) = A_m \cos\left(\frac{\gamma_m x}{a}\right) + B_m \sin\left(\frac{\gamma_m x}{a}\right) + C_m e^{-\frac{\gamma_m x}{a}} + D_m e^{-\frac{\gamma_m (a-x)}{a}}, \tag{10}$$

$$Y_n(x) = A_n \cos\left(\frac{\gamma_n y}{b}\right) + B_n \sin\left(\frac{\gamma_n y}{b}\right) + C_n e^{-\frac{\gamma_n y}{b}} + D_n e^{-\frac{\gamma_n (b-y)}{b}} \tag{11}$$

where a and b are the length and the width of the plate, respectively. A_m, A_n, B_m, B_n, C_m C_n, D_m D_n, γ_m, and γ_n are parameters dependent on the boundary conditions. For a fully clamped plate they take the values

$$A_m = A_n = A_r = 1, \qquad B_m = B_n = B_r = -\frac{1 + (-1)^r e^{-\gamma_r}}{1 - (-1)^r e^{-\gamma_r}}, \tag{12}$$

$$C_m = C_n = C_r = -\frac{1}{1 - (-1)^r e^{-\gamma_r}}, \quad D_m = D_n = D_r = \frac{(-1)^r}{1 - (-1)^r e^{-\gamma_r}} \tag{13}$$

where the parameters γ_r are given by solving the non-linear equation:

$$\cos(\gamma_r) - \frac{2e^{-\gamma_r}}{1 + e^{-2\gamma_r}} = 0 \tag{14}$$

It should be noted that since one has analytical functions as integrands in Equation (8) the computation of matrices $[K]$ and $[M]$ is performed analytically. Tests to compare the performance of numerical and analytical integrations showed that the latter is much more efficient than the former. For example, the computation of the matrices with the Simpson's rule is about forty times slower than the direct computation with analytical integrations.

2.1.2 Models of Damaged Orthotropic Laminated Plates

In this work, a reference finite element model of the damaged plate is created to simulate a complete set of measured data. Afterwards, based on this model, several others are generated in order to study the influence of incomplete sets of measurements and, therefore, the number of measured degrees of freedom in the quality of damage localisations using the present methods. These models are named as incomplete models [23]. They are built by deleting a set of degrees of freedom from the reference finite element model.

The damage is simulated by reducing the laminated stiffness $[D]$ of an element e of the undamaged plate such that the corresponding laminated stiffness of the damaged plate is given by:

$$\left\|[\widetilde{D}^{(e)}]\right\|_2 = \left(1 - d^{(e)}\right) \left\|[D^{(e)}]\right\|_2 \quad \text{with} \quad 0 \leq d^{(e)} \leq 1 \tag{15}$$

where the subscript 2 denotes the Frobenius norm of a matrix, given in is this case by:

$$\left\|[D^{(e)}]\right\|_2 = \sqrt{\left(D_{11}^{(e)}\right)^2 + \left(D_{22}^{(e)}\right)^2 + \left(D_{66}^{(e)}\right)^2 + 2\left(D_{12}^{(e)}\right)^2} \tag{16}$$

The parameter $d^{(e)}$ defines the amount of damage in the specified element. If $d^{(e)} = 0$ there is no reduction in the stiffness, whereas if $d^{(e)} = 1$ there will be a complete reduction of stiffness in element e. The SHELl finite element from the package FEAP is used [24]. It is a quadrilateral finite element with 4-nodes and six degrees of freedom (three translations and three rotations).

2.2 Damage Indicators

The damage indicators proposed are based on differences in modal displacement fields derivatives and are defined by the following expression:

$$DFD_i^{(p)}(x, y) = \left| \frac{\partial^p \widetilde{w}_i(x, y)}{\partial x^p} - \frac{\partial^p w_i(x, y)}{\partial x^p} \right| \tag{17}$$

with p denoting the order of the spatial derivative, i the mode shape, and x and y are the coordinates where these indicators are computed. The indicators of mode shape rotations and curvatures differences can be identified in Equation (17) with $p = 1$ and $p = 2$, respectively, if only one dimension is considered [3, 4]. Besides considering two dimensions, in the present work we also present results with $p = 3$ and $p = 4$.

One can take the sum of these damage indicators over n mode shape as follows:

$$SDFD^{(p)}(x, y) = \sum_{i=1}^{n} \left| \frac{\partial^p \widetilde{w}_i(x, y)}{\partial x^p} - \frac{\partial^p w_i(x, y)}{\partial x^p} \right| \tag{18}$$

Since the displacement field of the undamaged plate $w_i(x, y)$ is defined by a series expansion of known functions (see Equation (6)), the differentiations $\partial^p w_i(x, y)/\partial x^p$ in Equations (17) or (18) are performed analytically. However, the displacement of the damaged plate $\widetilde{w}(x, y)$ is obtained using the finite element method, and thus only discrete values are available. Therefore, a numerical differentiation technique to computed $\partial^p \widetilde{w}_i(x, y)/\partial x^p$ must be used. In the present work, the numerical technique chosen is the finite difference method. In reference [25] one finds several formulas of finite differences for a function of one variable and the associated approximation errors. All these finite differences can be extended to a function of two variables such as

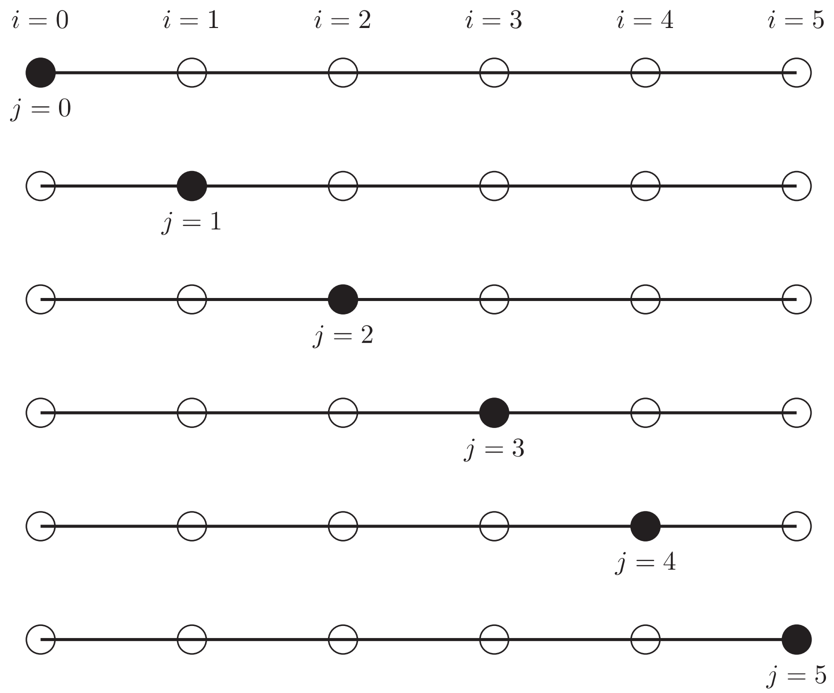

Figure 1: Point where the fourth derivative is computed ● and its neighbouring points ○ using six points finite difference formula

the one describing the displacement field of a plate. Therefore, the general expression for the computation of damaged displacement spatial derivatives in the x direction can be written as:

$$\frac{\partial^p \widetilde{w}(x_j, y)}{\partial x^p} \approx \frac{p!}{m! h_x^p} \sum_{i=0}^{m} P_i \widetilde{w}(x_i, y) \tag{19}$$

where m plus one is the number of points used in the approximation of $\widetilde{w}(x, y)$, (x_j, y) are the coordinates of the point where we are computing the derivative, (x_i, y) are coordinates of neighbouring points along a line with $y = \text{constant}$, such that $h_x = x_{i+1} - x_i$, and P_i are known coefficients. The coefficients P_i in Equation (19) are given in Appendix A in Tables A1, A2, A3 and A4 for the first, second, third and fourth derivatives, respectively. The approximation errors are also listed in these Tables. We see that the errors in the approximation of any p-th derivative is of order $\mathcal{O}(h_x^2)$.

Figure 1 shows the six possible positions of the point where the fourth derivative is computed using the six points finite difference. It can be seen that, by setting $j = 0$ or $j = 5$, i.e. by using backward or forward finite differences, the derivatives of points at the left and right edges of the plate can be computed. In a similar fashion, the same applies to the other order derivatives.

3 Results

The plate is 400 mm long, 200 mm wide and 2 mm thick and is clamped at all edges. The plate is a AS4/Epoxy, with the properties given in reference [26]. The layers stacking sequence is $[0, 90]_{3S}$. The undamaged mode shapes were computed using the Ritz method with $M = N = 26$ (see Equation (6)), and the eigenvectors are normalised to the mass matrix. The damaged mode shapes were computed using a finite element model (FEM) with 80×40 elements. Each element is a four nodes square element with a size of 5 mm and the total number of nodes is 81×41. The damage is a square area of 40 mm^2 and corresponds to 8×8 damaged elements. Two damage locations were considered: (a) L1, in the centre of the plate ($x_d = 200$ mm, $y_d = 100$ mm), and (2) L2, in the centre of the right upper quarter ($x_d = 300$ mm, $y_d = 150$ mm). The damage parameter $d^{(e)}$ is set to 0.1 (see Equation (15)). The eigenvectors of the damaged mode shapes are also normalised to the mass matrix.

Regarding the influence of incomplete sets of measurements, the models studied are characterised by the following number of nodes and distance h_x between two consecutive nodes:

- Model 0: 81×41 nodes, $h_x = 5$ mm (reference or complete model),
- Model 1: 41×21 nodes, $h_x = 10$ mm,
- Model 2: 21×11 nodes, $h_x = 20$ mm,
- Model 3: 11×6 nodes, $h_x = 40$ mm.

3.1 Complete Model

Figure 2 shows the first, second, third and fourth x-derivative of the first mode shape, computed using FEM data with finite differences and Ritz method data with analytical differentiation. It can be seen that for the FEM data, the higher the derivative, the higher the numerical noise. Since the derivatives of the Ritz method data are computed analytically there is no noise.

Some examples of using the different DFD indicators can be seen in Figures 3, 4 and 5. It is noticeable that the best order p of the x-derivative, and the corresponding DFD indicator, to localise the damage is different for each mode shape. Figure 3 shows the DFD indicators computed using the third mode shape, with the damage at locations L1 and L2. In this case, $p = 3$ and $p = 4$ present similar results in the localisation of damage. On the other hand, Figure 4 shows the DFD indicators computed using the fourth mode shape, being $p = 2$ and $p = 3$ the order of the x-derivative with better results. Figure 5 shows the DFD indicators computed using the eighteenth mode shape, where $p = 4$ is the best option to localise the damage.

The results of the damage localisation using the DFD indicators for each one of the first twenty modes and $p = 1$, 2, 3 and 4 are compiled in Table 1. It can be

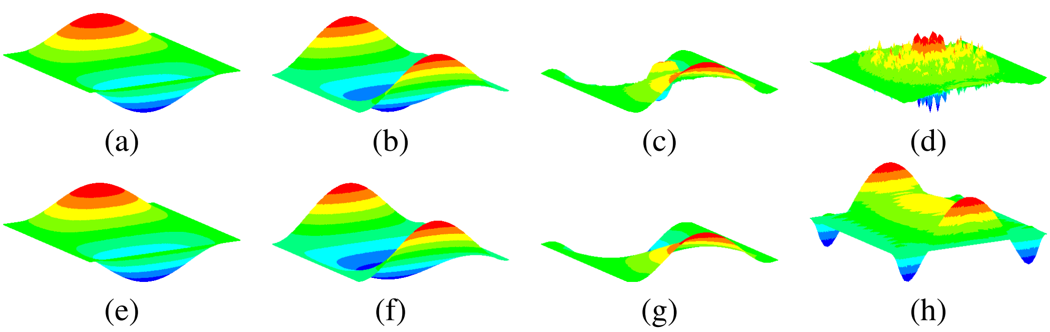

Figure 2: First (a, e), second (b, f), third (c, g) and fourth (d, h) x-derivative of first mode shape, computed with FEM data (damage location L1) and numerical differentiation (a-d) and the Ritz method data and analytical differentiation (e-h)

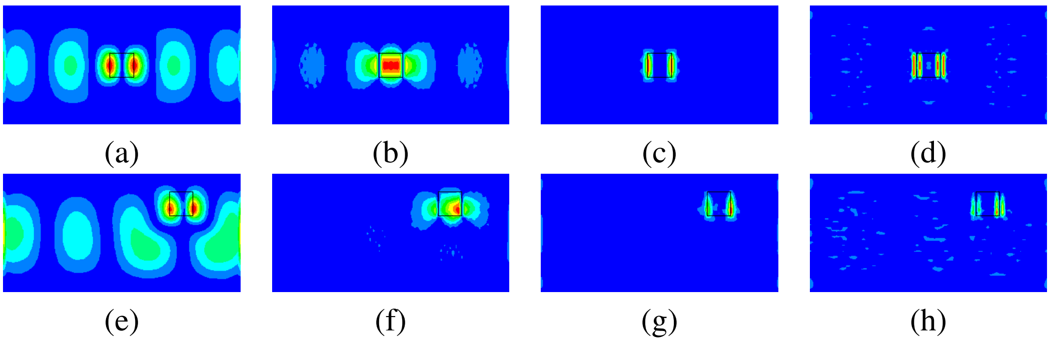

Figure 3: $DFD_3^{(1)}(x, y)$ (a, e), $DFD_3^{(2)}(x, y)$ (b, f), $DFD_3^{(3)}(x, y)$ (c, g) and $DFD_3^{(4)}(x, y)$ (d, h), with the damage at locations L1 (a-d) and L2 (e-h)

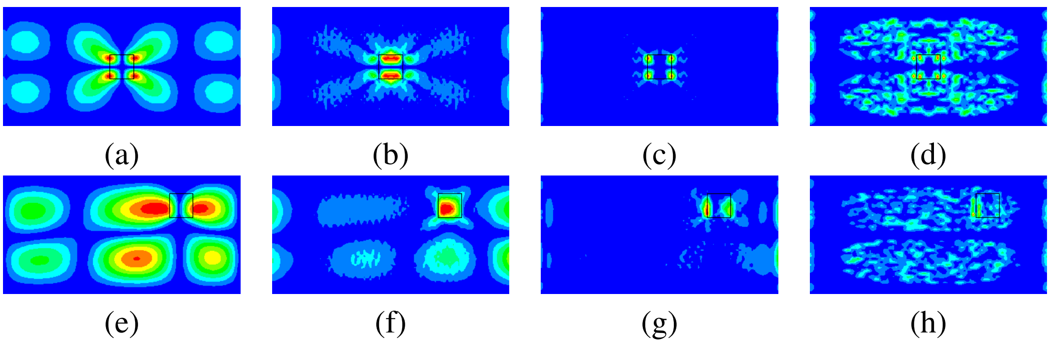

Figure 4: $DFD_4^{(1)}(x, y)$ (a, e), $DFD_4^{(2)}(x, y)$ (b, f), $DFD_4^{(3)}(x, y)$ (c, g) and $DFD_4^{(4)}(x, y)$ (d, h), with the damage at locations L1 (a-d) and L2 (e-h)

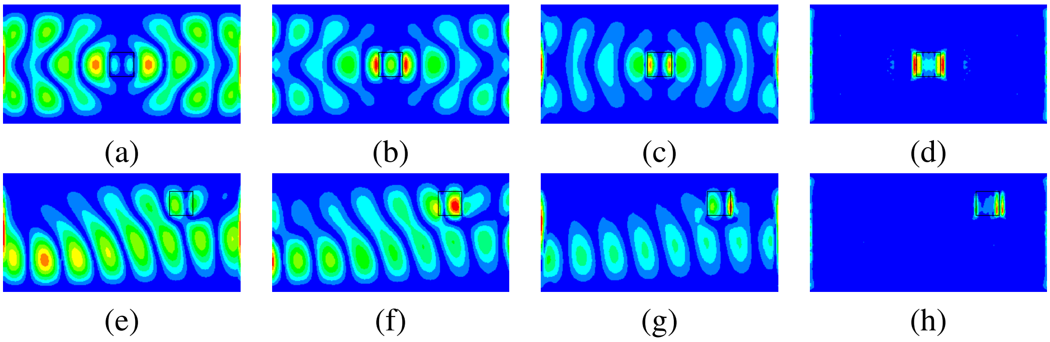

Figure 5: $DFD_{18}^{(1)}(x, y)$ (a, e), $DFD_{18}^{(2)}(x, y)$ (b, f), $DFD_{18}^{(3)}(x, y)$ (c, g) and $DFD_{18}^{(4)}(x, y)$ (d, h), with the damage at locations L1 (a-d) and L2 (e-h)

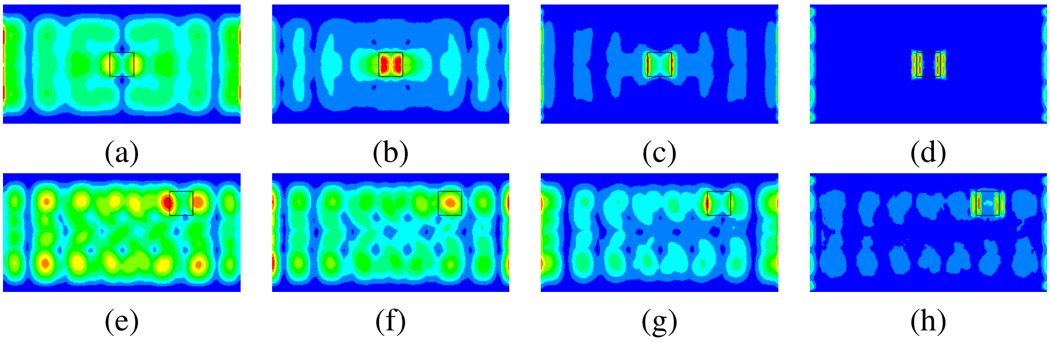

Figure 6: $SDFD^{(1)}(x, y)$ (a, e), $SDFD^{(2)}(x, y)$ (b, f), $SDFD^{(3)}(x, y)$ (c, g) and $SDFD^{(4)}(x, y)$ (d, h), all computed with $n = 20$, with the damage at locations L1 (a-d) and L2 (e-h)

seen that, in general, the higher the derivative, the higher the number of successful localisations of damage. Also, in general, the higher modes present better damage localisations than the lower ones.

Figure 6 shows the results of damage localisations with the $SDFD$ indicators, which are computed considering a sum over twenty modes ($n = 20$ in Equation (18)). Again, in general, the higher the derivative, the better the damage localisation.

3.2 Incomplete Models

Based on the results of the previous Section, only damage localisations with indicators based on the fourth derivative are reported here. Some examples of the DFD indicator using incomplete models can be seen in Figures 7 and 8. From Figure 7, an important conclusion can be made: some modes that are unsuccessful in locating the damage with the complete model can give good localisations with the incomplete models (first mode shape in this case). Figure 8 shows that for other modes, the reduction of the

Location	L1				L2			
p	1	2	3	4	1	2	3	4
Mode 1	Yes	Yes	Yes	No	Yes	Yes	No	No
Mode 2	Yes	Yes	Yes	No	Yes	Yes	Yes	Yes
Mode 3	Yes	Yes	Yes	Yes	Yes	Yes	Yes	Yes
Mode 4	Yes	No	Yes	No	No	Yes	Yes	No
Mode 5	Yes	No	No	No	Yes	Yes	Yes	Yes
Mode 6	No	Yes	Yes	Yes	No	Yes	Yes	Yes
Mode 7	Yes	No	Yes	Yes	No	Yes	Yes	Yes
Mode 8	No	No	No	Yes	Yes	Yes	Yes	Yes
Mode 9	Yes	Yes	Yes	Yes	No	Yes	Yes	Yes
Mode 10	No	No	No	Yes	Yes	Yes	Yes	Yes
Mode 11	No	No	No	No	No	No	No	No
Mode 12	Yes	Yes	Yes	No	Yes	Yes	Yes	Yes
Mode 13	No	No	Yes	Yes	No	No	No	Yes
Mode 14	No	Yes	Yes	Yes	No	No	No	Yes
Mode 15	No	No	Yes	Yes	No	Yes	Yes	Yes
Mode 16	No	Yes	No	Yes	No	No	No	Yes
Mode 17	No	No	No	Yes	No	No	Yes	Yes
Mode 18	No	No	No	Yes	No	No	No	Yes
Mode 19	No	Yes	Yes	Yes	No	No	No	No
Mode 20	No	No	No	Yes	No	No	No	No
Number of successful localisations	8	9	12	14	7	12	12	15

Table 1: Damage localisations using the $DFD_i^{(p)}$ indicators for each one of the first twenty mode shapes and $p = 1$, 2, 3 and 4, with the damage at locations L1 and L2

number of points causes a worsening in the damage localisation (third mode shape in this case).

A compilation of damage localisations with complete and incomplete models using the indicator $DFD_i^{(4)}$ for each one of the first twenty modes is presented in Table 2. It can be seen that, in general, a reduction in the number of measured points leads to less modes being able to successfully locate the damage, in particular for higher modes. However, it can be seen again that some modes that gave wrong results in the damage localisation with the complete model can give good results with incomplete models.

Regarding the $SDFD$ indicator, Figure 9 shows the results for this indicator computed with $n = 20$ and using the models 0, 1, 2 and 3. It can be seen that the damage indicator works worse when the number of points is decreasing. This is particularly noticeable with incomplete models 2 and 3, for which the damages are not located.

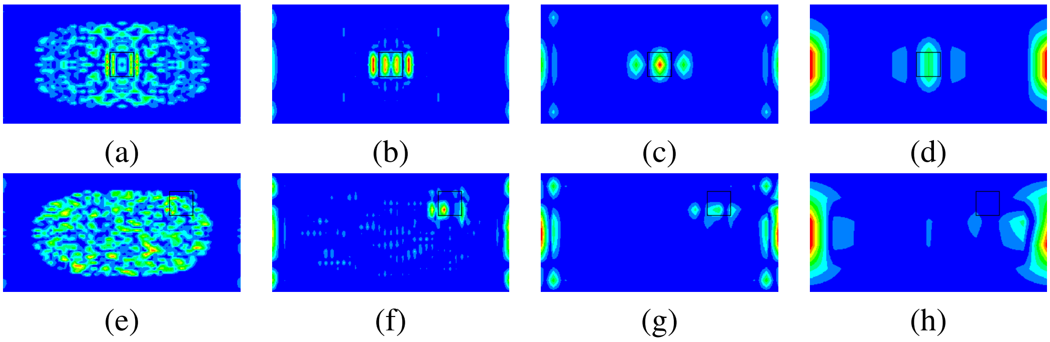

Figure 7: $DFD_1^{(4)}(x, y)$ using model 0 (a, e), model 1 (b, f), model 2 (c, g) and model 3 (d, h), with the damage at locations L1 (a-d) and L2 (e-h)

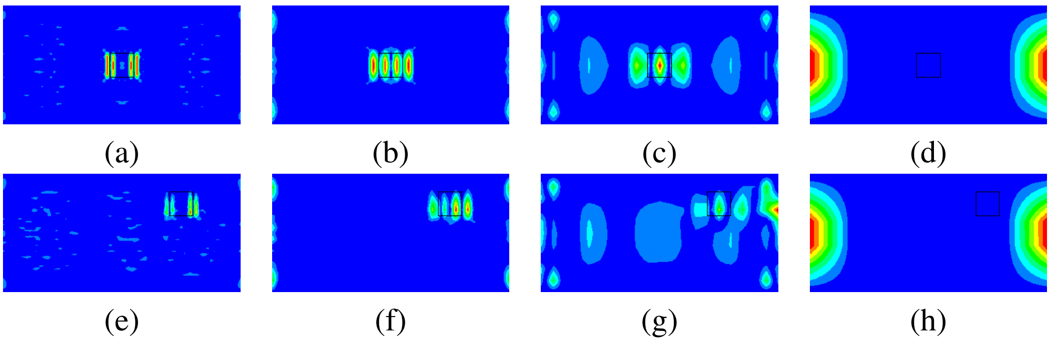

Figure 8: $DFD_3^{(4)}(x, y)$ using model 0 (a, e), model 1 (b, f), model 2 (c, g) and model 3 (d, h), with the damage at locations L1 (a-d) and L2 (e-h)

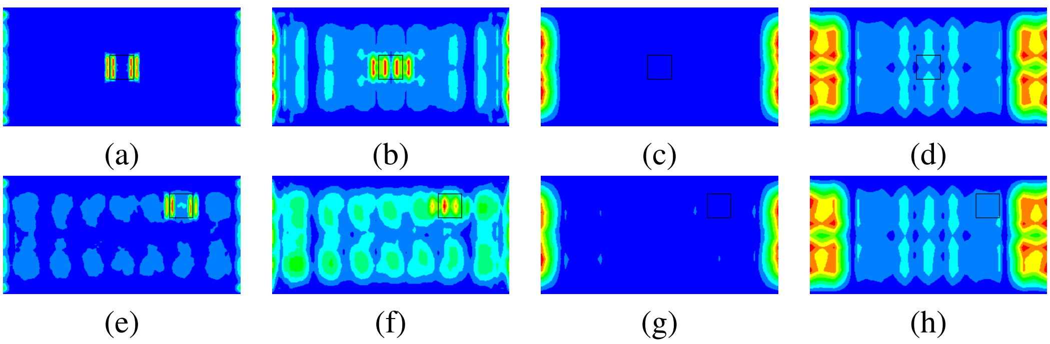

Figure 9: $SDFD^{(4)}(x, y)$ using model 0 (a, e), model 1 (b, f), model 2 (c, g) and model 3 (d, h), all computed with $n = 20$, with the damage at locations L1 (a-d) and L2 (e-h)

Location	L1				L2			
Model	0	1	2	3	0	1	2	3
Mode 1	No	Yes	Yes	Yes	No	Yes	Yes	No
Mode 2	No	Yes	Yes	No	Yes	Yes	Yes	No
Mode 3	Yes	Yes	Yes	No	Yes	Yes	Yes	No
Mode 4	No	Yes	Yes	No	No	Yes	Yes	Yes
Mode 5	No	Yes	No	No	Yes	Yes	Yes	No
Mode 6	Yes	Yes	No	No	Yes	Yes	No	No
Mode 7	Yes	Yes	No	No	Yes	Yes	Yes	No
Mode 8	Yes	Yes	No	No	Yes	Yes	No	No
Mode 9	Yes	Yes	No	No	Yes	Yes	No	No
Mode 10	Yes	No	No	No	Yes	Yes	No	No
Mode 11	No	Yes	Yes	No	No	Yes	No	No
Mode 12	No	Yes	No	No	Yes	Yes	Yes	No
Mode 13	Yes	Yes	Yes	No	Yes	Yes	No	No
Mode 14	Yes	Yes	No	No	Yes	No	No	No
Mode 15	Yes	Yes	No	No	Yes	Yes	No	No
Mode 16	Yes	No	No	No	Yes	No	No	No
Mode 17	Yes	No	No	No	Yes	Yes	No	No
Mode 18	Yes	No	No	No	Yes	No	No	No
Mode 19	Yes	No	No	No	No	No	No	No
Mode 20	Yes	No	No	No	No	No	No	No
Number of successful localisations	14	14	6	1	15	15	7	1

Table 2: Damage localisations using the $DFD_i^{(4)}$ indicator for each one of the first 20 modes and models 0, 1, 2 and 3, with the damage at locations L1 and L2

4 Conclusions

A set of new indicators for damage localisation in composite laminated plates using vibrational data are proposed in this paper. These indicators are defined as differences of third and fourth order spatial derivatives of modal displacement fields. The damaged displacement fields, generated with finite elements, are differentiated using higher order finite differences, whereas the undamaged displacement fields, computed using the Ritz method, are obtained analytically. Besides computing the damage indicators at interior points of the plate using central finite differences, the present method also computes these indicators at the plate edges by differentiating the displacement fields using forward and backward finite differences. Two damage cases are analysed and the results using all indicators show that they are mode shape dependent. Parametric studies carried out lead to the conclusion that, as the number of damaged measured degrees of freedom decrease, the success in damage localisation decreases.

It was also found that the damage indicator based on the fourth order spatial derivative of the modal displacement field allows better damage localisations, in particular by considering the sum of the differences of these derivatives over a certain number of modes shapes.

Acknowledgements

The authors greatly appreciate the financial support of FCOMP–01–0124–FEDER–010236 through Project Ref. FCT PTDC/EME–PME/102095/2008.

References

[1] J.V. Araújo dos Santos, N.M.M. Maia, C.M. Mota Soares, C.A. Mota Soares, *Structural damage identification: A survey*, pages 1–24, in Trends in computational structures technology, Saxe-Coburg Publications, Stirlingshire, UK, 2008.

[2] D. Montalvão, N.M.M. Maia, A.M.R. Ribeiro, "A review of vibration-based structural health monitoring with special emphasis on composite materials", *The Shock and Vibration Digest*, 38(4): 295–324, 2006.

[3] A.K. Pandey, M. Biswas, M.M. Samman, "Damage detection from changes in curvature mode shapes", *Journal of Sound and Vibration*, 145(2): 321–332, 1991.

[4] M.A. Abdo, M. Hori, "A numerical study of structural damage detection using changes in the rotation of mode shapes", *Journal of Sound and Vibration*, 251 (2): 227–239, 2002.

[5] N. Stubbs, J.T. Kim, C.R. Farrar, "Field verification of a nondestructive damage localization and severity estimator algorithm", in *Proc. 13th IMAC*, pages 210–218. Nashville, Tenessee, USA, 1995.

[6] R.P.C. Sampaio, N.M.M. Maia, J.M.M. Silva, "Damage detection using the frequency-response-function curvature method", *Journal of Sound and Vibration*, 226(5): 1029–1042, 1999.

[7] J. Maeck, G. Roeck, "Dynamic bending and torsion stiffness derivation from modal curvatures and torsion rates", *Journal of Sound and Vibration*, 225(1): 153–170, 1999.

[8] A. Dutta, S. Talukdar, "Damage detection in bridges using accurate modal parameters", *Finite Elements In Analysis and Design*, 40(3): 287–304, 2004.

[9] J.V. Araújo dos Santos, H.M.R. Lopes, M. Vaz, C.M. Mota Soares, C.A. Mota Soares, M.J.M. de Freitas, "Damage localization in laminated composite plates using mode shapes measured by pulsed TV holography", *Composite Structures*, 76(6): 272–281, 2006.

[10] N.M.M. Maia, J.V. Araújo dos Santos, R.P.C. Sampaio, C.M. Mota Soares, "Damage identification using curvatures and sensitivities of frequency-response-

functions", in A. Güemes (Editor), *Proc. Third European Workshop On Structural Health Monitoring 2006*, pages 547–554. Granada, Spain, July 5-7 2006.

[11] W. Lestari, P. Qiao, S. Hanagud, "Curvature mode shape-based damage assessment of carbon/epoxy composite beams", *Journal of Intelligent Material Systems and Structures*, 18(3): 189–208, 2007.

[12] H. Guan, V. Karbhari, "Improved damage detection method based on element modal strain damage index using sparse measurement", *Journal of Sound and Vibration*, 309(3–5): 465–494, 2008.

[13] M. Chandrashekhar, R. Ganguli, "Damage assessment of structures with uncertainty by using mode-shape curvatures and fuzzy logic", *Journal of Sound and Vibration*, 326(3–5): 939–957, 2009.

[14] A. Tomaszewska, "Influence of statistical errors on damage detection based on structural flexibility and mode shape curvature", *Computers & Structures*, 88 (3–4): 154–164, 2010.

[15] M. Radzienski, M. Krawczuk, M. Palacz, "Improvement of damage detection methods based on experimental modal parameters", *Mechanical Systems and Signal Processing*, 25(6): 2169–2190, 2011.

[16] T.M. Whalen, "The behavior of higher order mode shape derivatives in damaged, beam-like structures", *Journal of Sound and Vibration*, 309(3–5): 426–464, 2008.

[17] J.F. Gauthier, T.M. Whalen, J. Liu, "Experimental validation of the higher-order derivative discontinuity method for damage identification", *Structural Control and Health Monitoring*, 15(2): 143–161, 2008.

[18] J.V. Araújo dos Santos, H.M.R. Lopes, N.M.M. Maia, "A damage localisation method based on higher order spatial derivatives of displacement and rotation fields", *Journal of Physics: Conference Series*, 305: 012008, 2011.

[19] J.N. Reddy, *Mechanics of laminated composite plates and shells: Theory and analysis*, CRC Press, Boca Raton, Florida, 2004.

[20] J.V. Araújo dos Santos, A.L. Araújo, C.M. Mota Soares, "Eigenfrequency analysis of completely free multilayered rectangular plates using a higher order model and Ritz technique", *Mechanics of Composite Materials and Structures*, 5(5): 55–80, 1998.

[21] P. Frederiksen, "Single-layer plate theories applied to the flexural vibration of completely free thick laminates", *Journal of Sound and Vibration*, 186(5): 743–759, 1995, ISSN 0022-460X.

[22] J.R. Gartner, N. Olgac, "Improved numerical computation of uniform beam characteristic values and characteristic functions", *Journal of Sound and Vibration*, 84(4): 481–489, 1982.

[23] J.V. Araújo dos Santos, C.M. Mota Soares, C.A. Mota Soares, N.M.M. Maia, "Structural damage identification: influence of model incompleteness and errors", *Composite Structures*, 62(3–4): 303–313, 2003.

[24] R.L. Taylor, "FEAP – A finite element analysis program (Version 8.3 user manual)", URL `http://www.ce.berkeley.edu/projects/feap/manual.pdf`, (Accessed April, 5, 2012).

[25] M. Abramowitz, I.A. Stegun (Editors), *Handbook of mathematical functions with formulas, graphs, and mathematical tables*, Dover Publications, Inc., New York, 1972.
[26] D. Adams, L. Carlsson, R. Pipes, *Experimental characterization of advanced composite materials*, CRC Press, Boca Raton, Third edition, 2003.

Appendix A

This Appendix lists the coefficients P_i in Equation (19).

j	P_0	P_1	P_2	Error
0	-3	4	-1	$\frac{1}{3}\frac{\partial^3 w(\zeta,y)}{\partial x^3}h_x^2$
1	-1	0	1	$-\frac{1}{6}\frac{\partial^3 w(\zeta,y)}{\partial x^3}h_x^2$
2	1	-4	3	$\frac{1}{3}\frac{\partial^3 w(\zeta,y)}{\partial x^3}h_x^2$

Table A1: Coefficients P_i for the computation of first derivative ($p = 1$) with three points ($m = 2$) and $\mathcal{O}(h_x^2)$ approximation errors where $\zeta \in [x_0, x_m]$ [25]

j	P_0	P_1	P_2	P_3	Error
0	6	-15	12	-3	$\frac{11}{12}\frac{\partial^4 w(\zeta,y)}{\partial x^4}h_x^2$
1	3	-6	3	0	$-\frac{1}{12}\frac{\partial^4 w(\zeta,y)}{\partial x^4}h_x^2$
2	0	3	-6	3	$-\frac{1}{12}\frac{\partial^4 w(\zeta,y)}{\partial x^4}h_x^2$
3	-3	12	-15	6	$\frac{11}{12}\frac{\partial^4 w(\zeta,y)}{\partial x^4}h_x^2$

Table A2: Coefficients P_i for the computation of second derivative ($p = 2$) with four points ($m = 3$) and $\mathcal{O}(h_x^2)$ approximation errors where $\zeta \in [x_0, x_m]$ [25]

j	P_0	P_1	P_2	P_3	P_4	Error
0	-10	36	-48	28	-6	$\frac{7}{4}\frac{\partial^5 w(\zeta, y)}{\partial x^5}h_x^2$
1	-6	20	-24	12	-2	$\frac{1}{4}\frac{\partial^5 w(\zeta, y)}{\partial x^5}h_x^2$
2	-2	4	0	-4	2	$-\frac{1}{4}\frac{\partial^5 w(\zeta, y)}{\partial x^5}h_x^2$
3	2	-12	24	-20	6	$\frac{1}{4}\frac{\partial^5 w(\zeta, y)}{\partial x^5}h_x^2$
4	6	-28	48	-36	10	$\frac{7}{4}\frac{\partial^5 w(\zeta, y)}{\partial x^5}h_x^2$

Table A3: Coefficients P_i for the computation of third derivative ($p = 3$) with five points ($m = 4$) and $\mathcal{O}(h_x^2)$ approximation errors where $\zeta \in [x_0, x_m]$ [25]

j	P_0	P_1	P_2	P_3	P_4	P_5	Error
0	15	-70	130	-120	55	-10	$\frac{17}{6}\frac{\partial^6 w(\zeta, y)}{\partial x^6}h_x^2$
1	10	-45	80	-70	30	-5	$\frac{5}{6}\frac{\partial^6 w(\zeta, y)}{\partial x^6}h_x^2$
2	5	-20	30	-20	5	0	$-\frac{1}{6}\frac{\partial^6 w(\zeta, y)}{\partial x^6}h_x^2$
3	0	5	-20	30	-20	5	$-\frac{1}{6}\frac{\partial^6 w(\zeta, y)}{\partial x^6}h_x^2$
4	-5	30	-70	80	-45	10	$-\frac{5}{6}\frac{\partial^6 w(\zeta, y)}{\partial x^6}h_x^2$
5	-10	55	-120	130	-70	15	$\frac{17}{6}\frac{\partial^6 w(\zeta, y)}{\partial x^6}h_x^2$

Table A4: Coefficients P_i for the computation of fourth derivative ($p = 4$) with six points ($m = 5$) and $\mathcal{O}(h_x^2)$ approximation errors where $\zeta \in [x_0, x_m]$ [25]